

Comprehensive Analysis of Key Endoplasmic Reticulum Stress-Related Genes and Immune Infiltrates in Stanford Type A Aortic Dissection

ABSTRACT

Background: Type A aortic dissection is a fatal disease. However, the role of endoplasmic reticulum stress-related genes (ERSRGs) in type A aortic dissection has not yet been fully clarified.

Methods: Differentially expressed genes in the aorta of type A aortic dissection patients were analyzed based on the GSE52093 database. The ERSRGs were downloaded from the GeneCards website. Functional enrichment analysis and protein–protein interaction analysis were performed on the acquired differentially expressed ERSRGs. The mRNA expression of the 5 top key differentially expressed ERSRGs was further explored in GSE153434 and clinical samples. Immune infiltration correlation analysis was performed on the validated key genes. Finally, we constructed regulatory networks of transcription factors, miRNAs, and chemicals.

Results: Twelve differentially expressed ERSRGs were identified, of which 8 genes were downregulated and 4 genes were upregulated. GeneMANIA was adopted to analyze these genes and their interacting proteins, and the results showed that the main function was calcium ion transport. Four key genes, ACTC1, CASQ2, SPP1, and REEP1, were validated in GSE153434 and clinical samples. The area under the ROC curve values for ACTC1, CASQ2, SPP1, and REEP1 were 0.92, 0.96, 0.89, and 1.00, respectively. ACTC1 and REEP1 correlated with multiple immune cells. Many transcription factors, microRNAs, and chemicals were identified with the potential to regulate these 4 key genes.

Conclusion: In this study, we identified 12 differentially expressed ERSRGs by analyzing the Gene Expression Omnibus database. Four key genes may influence the development of type A aortic dissection by regulating endoplasmic reticulum stress. These results expand our understanding of type A aortic dissection, and the 4 key genes are expected to be diagnostic markers and potential therapeutic targets.

Keywords: Aortic dissection, gene ontology, gene expression profiling

ORIGINAL INVESTIGATION

INTRODUCTION

Aortic dissection (AD) is a fatal disease caused by the rupture of the aortic intima, which allows high-speed blood from the aortic lumen to enter the aortic wall through the rupture of the intima, resulting in tearing of the middle layer of the aortic wall.¹ The annual incidence rate of AD is 3.5–6 cases/100 000 people, but the mortality rate of AD is very high, often leading to sudden death.² According to the Stanford classification method, AD can be divided into type A aortic dissection (TAAD) and type B aortic dissection (TBAD).³ Currently, the main treatment for TAAD is emergency surgery with artificial vessel replacement, whereas the main treatment for TBAD is interventional thoracic endovascular aortic repair (TEVAR).⁴ Mortality is higher in the cases of TAAD, especially in areas with poorer health care.^{5,6} Therefore, there is a need for new drug development, which requires a deeper understanding of the molecular mechanisms underlying the pathogenesis of TAAD.

The endoplasmic reticulum (ER) controls the quality of the proteins it produces and oversees maintaining protein homeostasis, which is critical for cell survival. Protein imbalances can lead to a variety of diseases, including metabolic,

Wei Zhou 

Jun Nie 

Dafa Zhang 

Department of Cardiothoracic Surgery,
The First Affiliated Hospital of Wannan
Medical College, Wuhu, China

Corresponding author:

Dafa Zhang

✉ zhangdafa2256@126.com

Received: January 9, 2024

Accepted: February 7, 2024

Available Online Date: March 5, 2024

Cite this article as: Zhou W, Nie J, Zhang D. Comprehensive analysis of key endoplasmic reticulum stress-related genes and immune infiltrates in stanford type A aortic dissection. *Anatol J Cardiol.* 2024;28(5):236–244.



Copyright©Author(s) - Available online at anatoljcardiol.com.
Content of this journal is licensed under a Creative Commons Attribution-NonCommercial 4.0 International License.

DOI:10.14744/AnatolJCardiol.2024.4251

oncological, neurodegenerative, and cardiovascular diseases.^{7,8} Under special circumstances, the normal oxidative environment within the intracellular ER is altered by specific strikes such as hypoxia and drug toxicity, calcium metabolism is disturbed, ER function is dysfunctional, and misfolded or unfolded proteins accumulate within the ER, known as endoplasmic reticulum stress (ERS).^{9,10} Previous studies have shown that ERS plays a certain role in tumors, vascular calcification disease, liver steatosis, diabetes, and ischemic heart failure. However, the role of endoplasmic reticulum stress-related genes (ERSRGs) in TAAD disease has not yet been fully clarified.¹¹⁻¹⁶

In this study, we analyzed differentially expressed ERSRGs in TAAD based on the GEO database. Four key ERSRGs were identified and validated by quantitative reverse transcription PCR (qRT-PCR). The results of this study expand our understanding of TAAD and provide new potential diagnostic markers and potential therapeutic targets.

METHODS

Artificial Intelligence Statement

We confirmed that we did not use artificial intelligence or any assisted technologies such as large language models in this paper.

Data Source

The Gene Expression Omnibus (GEO) database (<https://www.ncbi.nlm.nih.gov/geo/>) is a public functional genomics database. We utilized the keywords "aortic dissection" to search in the GEO database. The inclusion criteria for datasets were as follows: (1) The datasets must include TAAD and normal control aortic specimens and (2) the number of aortic dissection samples and normal control samples in the dataset must be greater than 5 cases. In the end, 2 aortic coarctation mRNA expression profiles, GSE52093 and GSE153434, were included in this study. The GSE52093 dataset (GPL10558 platform) contained 7 aortic specimens of TAAD and 5 normal control aortic specimens,¹⁷ and GSE153434 (GPL20795 platform) contained 10 aortic specimens of TAAD and 10 normal control aortic specimens.¹⁸

Analysis of Differentially Expressed Genes

We downloaded the dataset from the GEO database through the R software GEO query package using the limma package to standardize the data. The results of the analysis of differentially expressed genes (DEGs) were visualized by volcano plots using the ggplot2 R package,¹⁹ with the setting

of $|\log \text{fold change (FC)}| > 1$ and an adjusted P value $< .05$. The significantly expressed genes were then visualized by heatmap using the ComplexHeatmap package.²⁰

Identification of Differentially Expressed Endoplasmic Reticulum Stress-Related Genes

Following the methods reported in the previous literature,²¹ we downloaded the ERSRGs from the GeneCards website, obtaining 1350 genes. These genes were intersected with differential genes obtained by GSE52093 to obtain differentially expressed ERSRGs in TAAD. Then, we plotted Venn plots.

Functional Enrichment Analysis and Protein-Protein Interaction

To explore the functions and metabolic pathways of differentially expressed ERSRGs, we conducted functional enrichment analysis using Metascape (version 3.5) (<https://metascape.org/gp/index.html#/main/step1>). We input differentially expressed ERSRGs into the GeneMANIA database (<http://genemania.org/>), which automatically performs protein-protein interaction (PPI) analysis.²²

Immune Infiltration Analysis

Based on the GSE153434 dataset, immune infiltration in aortic wall tissue of TAAD patients was calculated by applying the R software CIBERSORT [v1.03] R package. Twenty-two markers of immune cells were provided by the CIBERSORTx website (<https://cibersortx.stanford.edu/>).²³

Construction of the Regulatory Network

Transcription factors (TFs) and microRNAs (miRNAs) have inhibitory and regulatory effects on target genes. Based on the NetworkAnalyst online database (<https://www.networkanalyst.ca/NetworkAnalyst/>), we constructed gene-miRNA and gene-TF regulatory networks for differentially expressed ERSRGs.²⁴ Simultaneously, we searched this database and set the search source as the Comparative Toxicogenomics Database (CTD) to construct the gene-chemical network.

Clinical Specimen Collection and Quantitative Reverse Transcription Polymerase Chain Reaction Validation

The inclusion criteria for TAAD cases were as follows: clearly diagnosed TAAD by aortic CTA angiography and underwent aortic vascular replacement surgery, aged over 18 years old. The exclusion criteria were as follows: Combined connective tissue disease, severe infection, or malignant tumor. Inclusion criteria for coronary artery bypass grafting cases: those who underwent coronary artery bypass grafting surgery due to coronary heart disease. Exclusion criteria: combined connective tissue disease, severe infection, or malignant tumor. This study included a total of 24 clinical specimens of the ascending aorta to further validate the differentially expressed ERSRGs: 12 TAAD patients who underwent aortic vascular replacement (AD group) and 12 coronary artery bypass grafting patients (aortic wall tissue at the site of ascending aortic perforation for graft vessel) as a non-AD control group (NAD group). The study was performed in accordance with the Declaration of Helsinki. All study protocols and experiments were approved by the Ethics Committee of The First

HIGHLIGHTS

- The role of endoplasmic reticulum stress-associated genes (ERSRGs) in TAAD has not yet been fully clarified.
- Twelve differentially expressed ERSRGs in TAAD were identified by analyzing the GEO database.
- Four key genes (ACTC1, CASQ2, SPP1, and REEP1) were validated in GSE153434 and clinical samples, which are expected to be diagnostic markers and potential therapeutic targets of TAAD.

Table 1. Primer Sequences for Quantitative Reverse Transcription Polymerase Chain Reaction

Primers	Sequence, 5'–3'
β-Actin	F:AGCGAGCATCCCCCAAAGTT; R:GGGCACGAAGGCTCATCATT
ACTC1	F: TCCCATCGAGCATGGTATCAT; R: GGTACGGCCAGAAGCATACA
CASQ2	F: GGCAGAAGAGGGGCTTAATTT; R: GAAGACACCGGCTCATGGTAG
SPP1	F: CTCCATTGACTCGAACGACTC; R: CAGGTCTGCGAACTTCTTAGAT
REEP1	F: GGACAGGGTGCCTTATCGG R: ACTCCTGGACATCTTAGGCTG

Affiliated Hospital of Wannan Medical College, and prior informed consent was signed by the participants.

Total RNA was extracted from aortic wall tissue using TRIzol reagent (Invitrogen Company), and mRNA reverse transcription was performed using Vazyme’s HiScript II Q RTsuperMix for qPCR (+gDNA wiper) kit (R223-01). qRT-PCR was performed using the AceQ qPCR SYBR Green Master Mix kit (Q111-02103), with the primer sequences shown in Table 1. Relative quantification was calculated using the 2^{-ΔΔCT} method.

Statistical Analysis

Continuous variables are presented as the mean and standard deviation. The statistical analysis of bioinformatics data in this study was conducted using R software (<https://www.r-project.org/>, version 4.2.1).²⁵ Statistical analysis was conducted on differences in gene expression levels using Prism 9 software and Student’s t-test. The diagnostic significance of differentially expressed ERSRGs in TAAD patients was evaluated using receiver operating characteristic curves (ROC) and the area under the ROC curve (AUC). All tests were considered statistically significant with *P* < .05.

RESULTS

Analysis of Differentially Expressed Genes

The analysis was based on the GSE52093 dataset. The normalized sample data is shown in Figure 1A, while the PCA plot is shown in Figure 1B. After the analysis of DEGs (|log fold change (FC)|>1, adjusted *P* value <.05), we plotted volcano maps (Figure 1C) and heatmaps (Figure 1D), and obtained a total of 160 DEGs, including 94 upregulated genes and 66 downregulated genes (Supplementary File S1).

Identification of Differentially Expressed Endoplasmic Reticulum Stress-Related Genes

Twelve differentially expressed ERSRGs were obtained by taking the intersection of GSE52093 with the ERSRGs downloaded from the GeneCards website: ACTC1, CASQ2, REEP1,

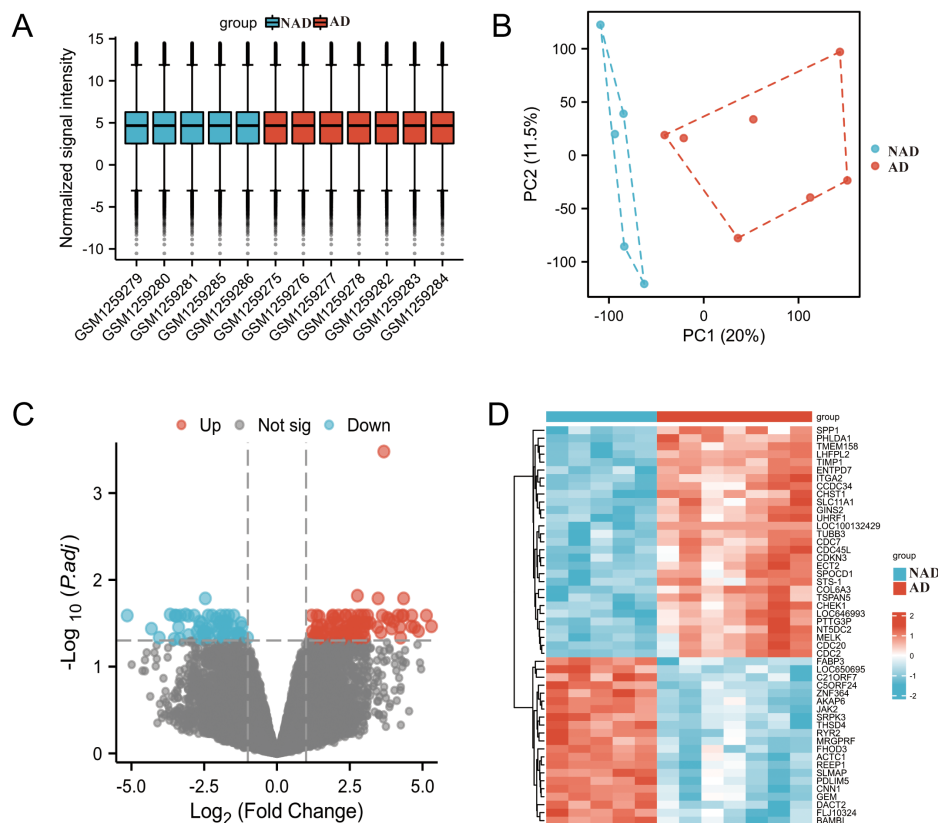


Figure 1. Differentially expressed gene (DEG) analysis based on GSE52093. A. Box plot of normalized samples. B. Principal component analysis. C. The volcano plot for the DEGs. Upregulated genes were represented by red points, whereas downregulated genes were represented by blue points. Genes with no significant difference (NS) were indicated by black dots. (D) The DEG heatmap.

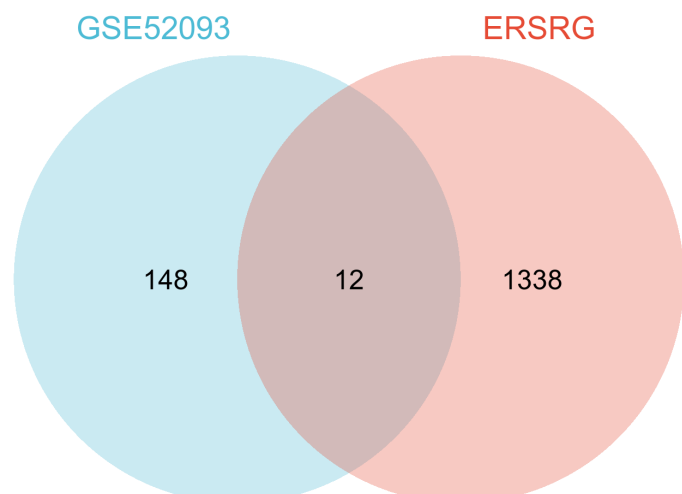


Figure 2. Venn diagram of the differentially expressed endoplasmic reticulum stress-related genes.

AKAP6, RYR2, JAK2, CAMK2G, WFS1, SERPINH1, CHEK1, CDKN3, SPP1, and CDKN3 (Figure 2, Table 2).

Functional Enrichment Analysis

Based on the Metascape database, we conducted a functional enrichment analysis of the 12 ERSRGs obtained. The 5 most significantly enriched GO terms and KEGG pathways were identified: (1) cellular response to caffeine; (2) negative regulation of molecular function; (3) Signaling by receptor tyrosine kinases; (4) supramolecular fiber organization; and (5) regulation of growth (Figure 3).

PPI Analysis

GeneMANIA was used to analyze 12 differentially expressed ERSRGs and their interacting proteins, and the results

Table 2. The 12 Endoplasmic Reticulum Stress-Related Genes in Type A Aortic Dissection

Gene	Log FC	P	Adj. P	Changes
ACTC1	-5.1444348	1.3893E-05	.02576853	Down
CASQ2	-4.0428139	.00018377	.04632685	Down
REEP1	-3.6678588	4.4556E-06	.02508415	Down
AKAP6	-3.1371289	4.9201E-06	.02508415	Down
RYR2	-2.4615297	2.0377E-06	.01637688	Down
JAK2	-1.7785296	1.1183E-05	.02576853	Down
CAMK2G	-1.7393782	.00010704	.03935819	Down
WFS1	-1.3206888	.00014406	.04165051	Down
SERPINH1	2.05872208	5.0329E-05	.03139493	Up
CHEK1	2.99801227	2.1524E-05	.02576853	Up
SPP1	3.79791129	2.7459E-05	.02739081	Up
CDKN3	3.86285789	3.0561E-05	.02861835	Up

are shown in Figure 4, whose main function is calcium ion transport.

Validation in GSE153434

To evaluate the veracity of the differentially expressed ERSRGs in TAAD, we used GSE153434 to validate the expression levels of the top 5 ($|\log FC|$) differentially expressed ERSRGs: ACTC1, CASQ2, CDKN3, SPP1, and REEP1. The expression levels of ACTC1, CASQ2, and REEP1 were significantly decreased in the AD group compared with the NAD group. In addition, the expression level of SPP1 was significantly increased in the AD group. However, the expression level of CDKN3 showed no significant difference between the 2 groups (Figure 5A). Area under the curve values for ACTC1, CASQ2, SPP1, and REEP1 were 0.92, 0.96, 0.89, and 1.00, respectively (Figure 5B).

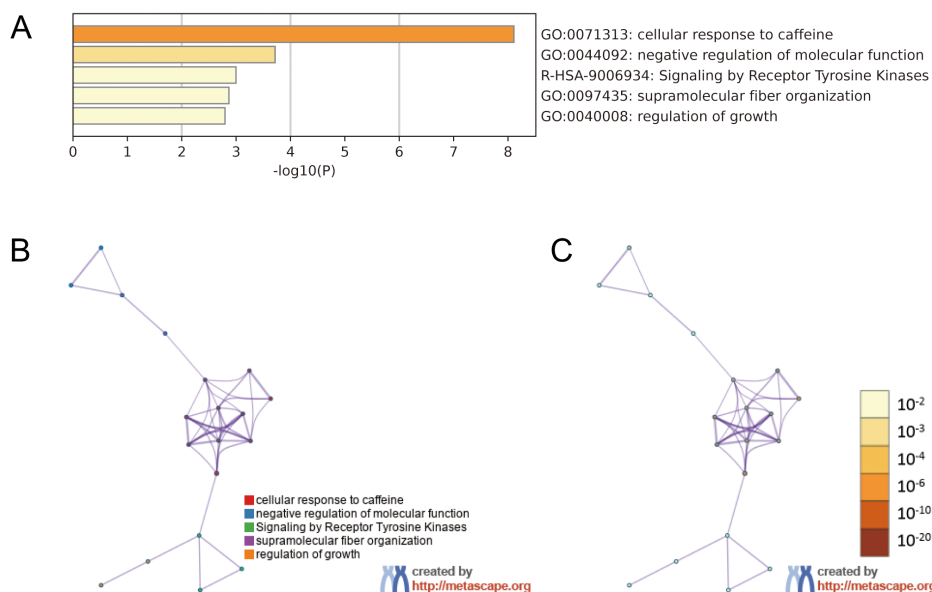


Figure 3. Functional enrichment analysis of 12 differentially expressed ERSRGs in TAAD. (A) Bar graph of enriched terms, colored by P value. (B) Network of enriched terms colored by cluster ID, where nodes that share the same cluster ID are typically close to each other. (C) Network of enriched terms colored by P value. ERSRGs, endoplasmic reticulum stress-related genes; TAAD, type A aortic dissection.

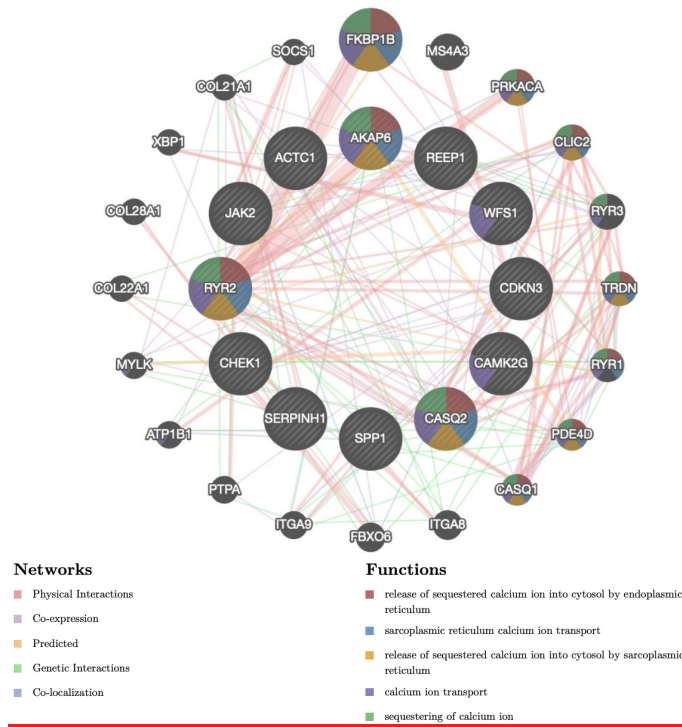


Figure 4. Protein-protein interaction analysis.

Validation in Clinical Samples

We examined the expression of ACTC1, CASQ2, SPP1, and REEP1 using qRT-PCR in the AD (n=12) and NAD (n=12) groups of clinical samples, and the results again demonstrated that ACTC1, CASQ2, and REEP1 were expressed at low levels in TAAD, while SPP1 was highly expressed in TAAD, and the difference was statistically significant (Figure 6).

Immune Infiltrate Analysis

To assess the correlation between the 4 validated ERSRGs and immune infiltrating cells, we analyzed the distribution ratio of 22 types of immune cells within the TAAD aortic wall tissue based on the GSE153434 dataset (Figure 7A). Correlation analysis among various immune cells was also performed (Figure 7B), which showed that T cells CD8 were positively correlated with Treg cells and dendritic cells resting. Treg cells were positively correlated with dendritic cells resting. While NK cells activated were negatively correlated with macrophages M2 ($P < .05$). The expression of ACTC1 was negatively correlated with T cells CD8 and NK cells activated, and negatively correlated with NK cells resting (Figure 7C). The expression of REEP1 was negatively correlated with NK cells resting (Figure 7F). However, the expression of CASQ2 and SPP1 had no significant correlation with immune cell infiltration (Figure 7D,E).

Construction of Regulatory Networks

Then, we built the gene-miRNA (Figure 8A) and gene-TF regulatory networks (Figure 8B) of ACTC1, CASQ2, SPP1, and REEP1. The results revealed that a number of miRNAs and TFs were involved in the regulation of these 4 genes. We also built gene-chemical regulatory networks (Figure 8C), and the results suggested that multiple chemicals could regulate these 4 genes. These chemicals have the potential for the treatment of TAAD.

DISCUSSION

Type A aortic dissection is a serious life-threatening disease that requires prompt diagnosis and emergency surgical treatment. However, the molecular mechanisms underlying its pathogenesis are still not fully elucidated. In this study, we included and analyzed 2 GSE datasets and identified 12 differentially expressed ERSRGs, and ACTC1, CASQ2, SPP1, and

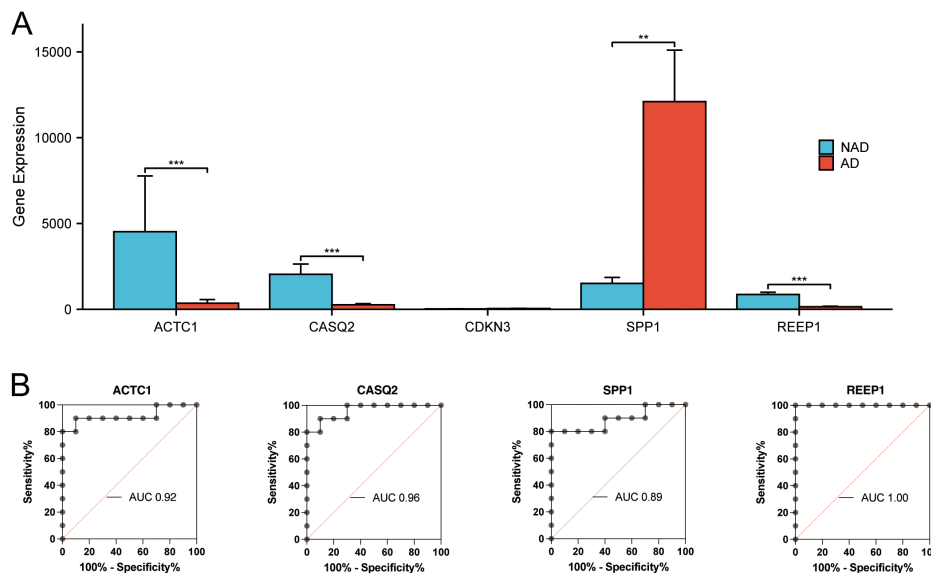


Figure 5. Validation of the top 5 differentially expressed ERSRGs in GSE153434. (A) The gene expression levels of ACTC1, CASQ2, CDKN3, SPP1, and REEP1. (B) ROC curves of ACTC1, CASQ2, SPP1, and REEP1. $P < .01$, and $***P < .001$. ERSRGs, endoplasmic reticulum stress-related genes.**

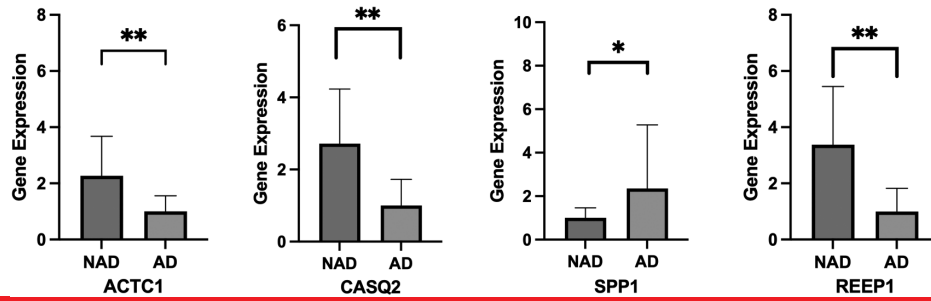


Figure 6. Validation of ACT1, CASQ2, SPP1, and REEP1 expression levels using quantitative reverse transcription polymerase chain reaction in clinical samples. * $P < .05$, ** $P < .01$.

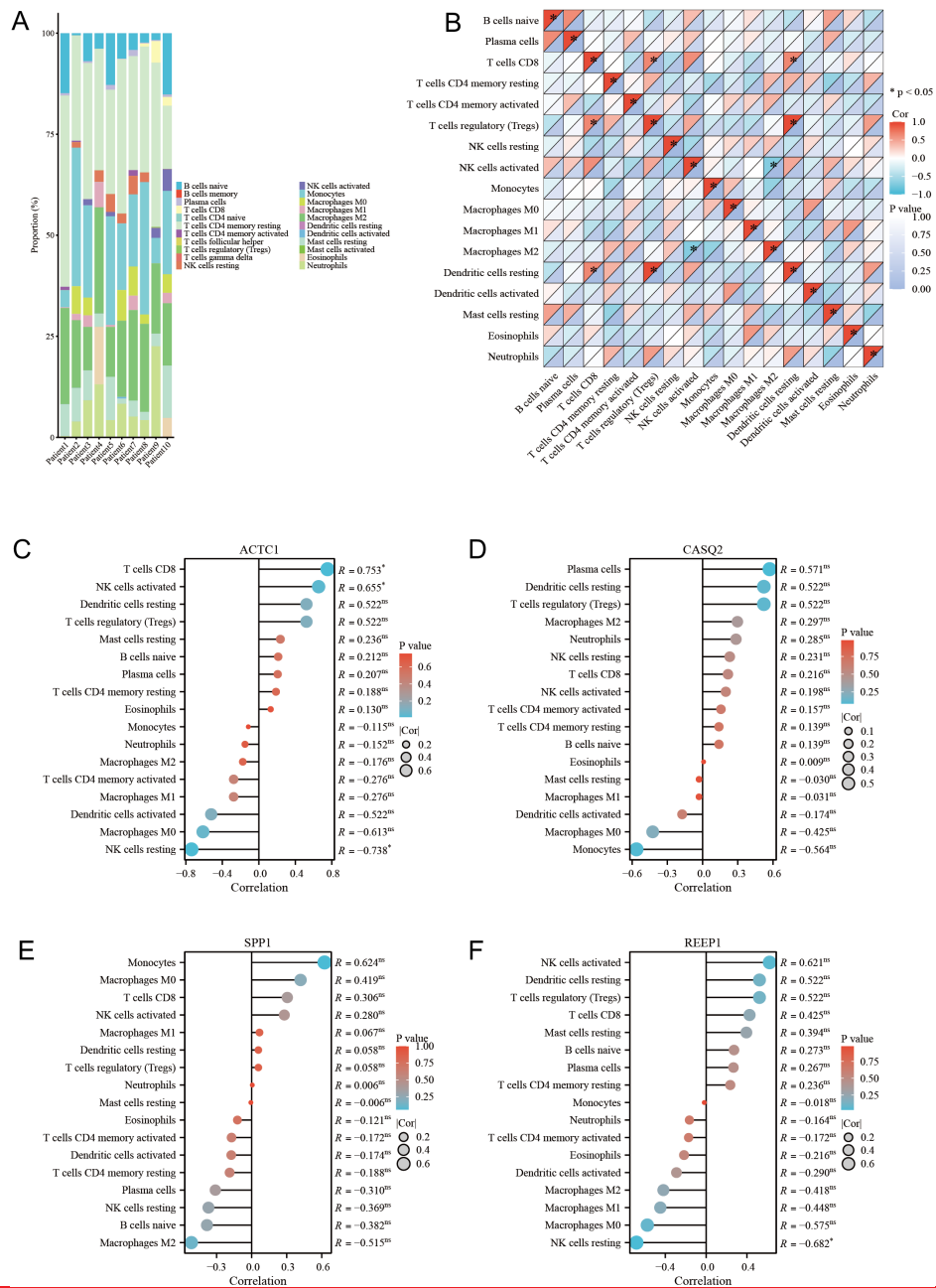


Figure 7. Immune cell infiltration analysis based on GSE153434. (A) The proportions of 22 different kinds of infiltrating immune cells in TAAD samples. (B) Correlation analysis of the 22 different immune cell types. (C–F) Correlation analysis of ACT1, CASQ2, SPP1, and REEP1 with 22 types of immune cells. Pearson method, * $P < .05$. TAAD, type A aortic dissection.

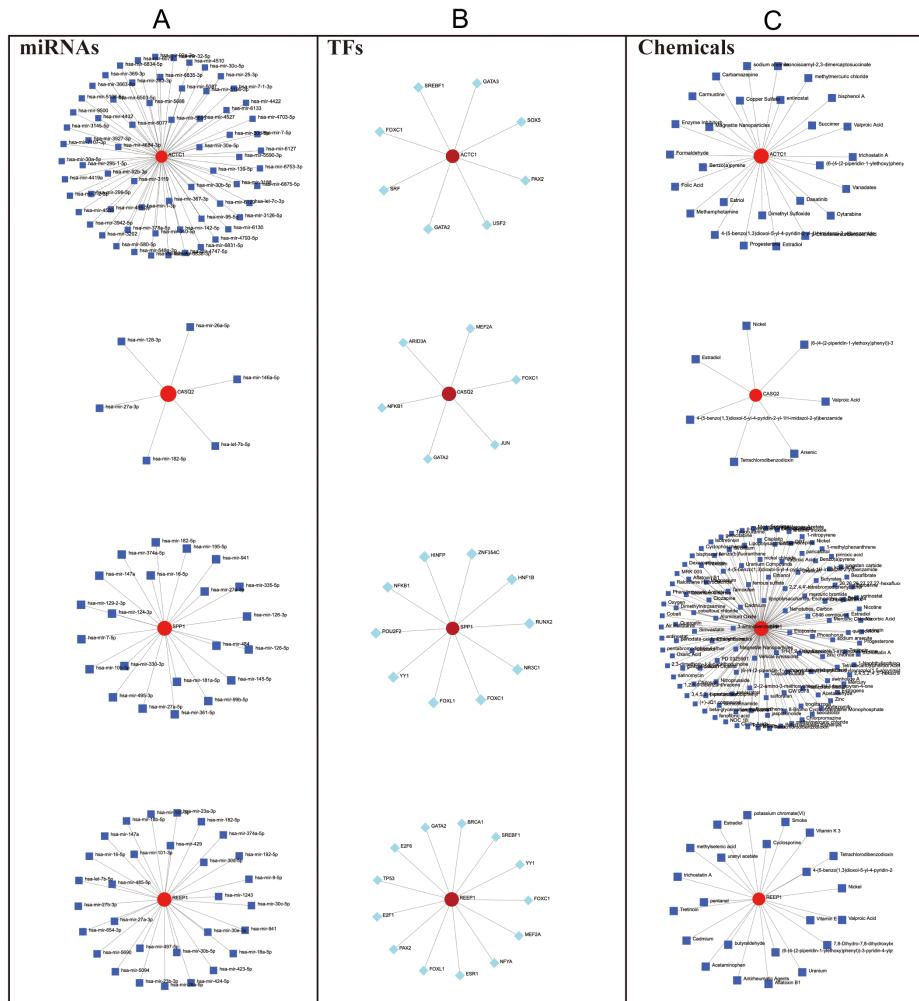


Figure 8. Construction of the regulatory networks of ACTC1, CASQ2, SPP1, and REEP1. (A) The gene–miRNA regulatory network. (B) The regulatory networks of gene–TF. (C) The gene–chemical regulatory networks.

REEP1 were validated in clinical specimens. To further understand the possible role of these 4 differentially expressed ERSRGs, we analyzed their correlation with immune cell infiltration. Our study suggests that the 4 differentially expressed ERSRGs can serve as biomarkers for TAAD diagnosis and potential therapeutic targets.

Endoplasmic reticulum stress is closely associated with tumors, myocardial injury, and other diseases. Previous studies have demonstrated that ATF3 attenuates myocardial injury by regulating SPHK1 through the ERS pathway.²⁶ In colon cancer, oridonin increases cancer cell death via TP53-promoted ERS.²⁷ In this study, 4 differentially expressed ERSRGs, ACTC1, CASQ2, SPP1, and REEP1, were identified and validated. In cardiomyocytes and skeletal muscle, calsequestrin 2 (CASQ2) was found in the intracellular endoplasmic reticulum or sarcoplasmic reticulum and binds to calcium.²⁸ Catecholaminergic polymorphic ventricular tachycardia can be caused by homozygous point mutations in CASQ2.²⁹ CASQ2 controls the intracellular calcium concentration, which in turn modulates muscular contraction and activates cardiomyocytes. Additionally, ryanodine receptor 2 (RYR2) allows CASQ2, the main calcium reservoir protein

in the heart, to release calcium into the cytosol in response to changes in calcium concentration.³⁰ RYR2 activity in myocytes is linked to electrical and contractile failure in the arrhythmogenic heart of an elderly person via mitochondrial function, calcium homeostasis, and excitation–contraction coupling.³¹ In the present study, we found lower expression of CASQ2 in TAAD patients and further validated this finding in clinical specimens. Our results suggest that alterations in calcium channels may influence the development of TAAD.

SPP1, also known as osteopontin, has previously been linked to degenerative aneurysmal illness, including abdominal aortic aneurysms,³² and has been demonstrated to play a role in a variety of blood vessel diseases.³³ SPP1, for example, is produced during inflammation and binds to transmembrane ligands to influence tissue remodeling pathways.³⁴ Furthermore, SPP1 participates in cellular migration, proliferation, apoptosis, and macrophage chemotaxis.³⁵ Previous research has linked SPP1 to abdominal and thoracic aneurysmal illness by upregulating matrix proteinases via NF- κ B, increasing tissue degradation.^{36,37} A previous study showed that individuals with abdominal aortic aneurysm and AD had higher levels of SPP1 expression in the plasma and aortic wall

than healthy controls. In AD patients, serum SPP1 levels correlate positively with MMP-2 levels. Thus, SPP1 is thought to be important in the development of aortic aneurysm and dissection.³⁸ Our findings suggest that REEP1 is highly expressed in TAAD, which is consistent with previous findings.

Expression-enhancing protein 1 (REEP1) is one of the proteins that make up mitochondria-associated endoplasmic reticulum membranes (MAM). Abnormalities in MAM proteins often lead to the incidence and progression of associated disorders such as diabetic kidney disease, neurodegenerative diseases, and type 2 diabetes mellitus.³⁹ The correlation between REEP1 and TAAD has not been previously reported, and we believe that the downregulation of REEP1 may be related to the development of TAAD, which needs to be further investigated in future experiments.

Vascular inflammation is a major contributor to the development of AD. Many studies have shown that a cascade of cytokines and inflammatory cells plays a role in disease progression. For example, the cytokine IL33 is an efficient AD diagnostic marker.⁴⁰ In addition to cytokines, inflammatory cells pass across the compromised endothelial tight connections, causing vascular inflammation and, eventually, AD.⁴¹ Endoplasmic reticulum stress is associated with a variety of pathological conditions associated with chronic inflammation, which can trigger inflammatory pathways and proinflammatory stimuli such as Toll-like receptor ligands, reactive oxygen species, and cytokines. These proinflammatory signals can initiate ERS and lead to activation of the unfolded protein response, which further amplifies the inflammatory response.⁴² Immunoinflammation-related mechanisms play an important role in AD disease, for example, in animal models, neutrophil-secreted MMP9 can induce AD.⁴³ Previous studies have shown that aortic arterial wall remodeling depends on complex interactions between cells, proinflammatory mediators, and MMPs, which are regulated by immune responses.^{44,45} Treg cells will be significantly inhibited in immune cell activation response after blockade by CD25 monoclonal antibody, and IL-10 immunoreactivity will be abnormal, which in turn promotes aortic aneurysm development AD.⁴⁶ Previous studies have suggested that SPP1 is associated with macrophage recruitment in AD disease.⁴⁷ In our study, we found a correlation between ACTC1 and REEP1 and immune cell infiltration, however, CASQ2 and SPP1 did not show a significant correlation with immune cells, which may be due to the small sample size of the enrolled GEO dataset.

However, this study still has some limitations. First, clinical validation with large samples was lacking, and second, animal models were not constructed to study the specific molecular mechanisms of these genes. These limitations will be solved in our future research work.

CONCLUSION

In this study, we identified 12 differentially expressed ESRGs by analyzing the GEO database. Four key differentially expressed ESRGs may influence the development of TAAD by regulating ERS. These results expanded our understanding

of TAAD, and the 4 genes are expected to be diagnostic markers and potential therapeutic targets.

Ethics Committee Approval: This study was performed according to the ethical standards of the responsible committee on human experimentation (institutional and national) and with the Helsinki Declaration of 1975, as revised in 2000. All study protocols and experiments were approved by the Ethics Committee of The First Affiliated Hospital of Wannan Medical College (Ethics No.: 2021-02).

Informed Consent: Written informed consent was obtained from the patients who agreed to take part in the study.

Peer-review: Externally peer-reviewed.

Author Contributions: Concept – W.Z.; Design – W.Z., D.Z.; Supervision – W.Z., J.N.; Resources – W.Z., J.N.; Materials – W.Z., D.Z., J.N.; Collection and/or Processing – J.N.; Analysis and/or Interpretation – W.Z.; Literature Search – D.Z., J.N.; Writing – W.Z.; Critical Review – D.Z.

Acknowledgements: The authors thank the researchers of the enrolled GEO dataset.

Declaration of Interests: The authors have no conflicts of interest to declare.

Funding: This research was supported by the Special Start-up Research Fund for Introducing Talents to the First Affiliated Hospital of Wannan Medical College (YR20230106), the Translational Research of Non-coding RNA for Major Diseases of Wannan Medical College (No. RNA202009), and Clinical Medical Research Translation Special Program of Anhui Province (No. 202304295107020002).

REFERENCES

- Mussa FF, Horton JD, Moridzadeh R, Nicholson J, Trimarchi S, Eagle KA. Acute Aortic Dissection Intramural Hematoma. *JAMA*. 2016;316(7):754-763.
- Chiu P, Miller DC. Evolution of surgical therapy for Stanford acute type A aortic dissection. *Ann Cardiothorac Surg*. 2016;5(4):275-295. [CrossRef]
- Huai H, Wu H, Chen Y, Zhang N, Fan Z. Early detection of post-operative acute kidney injury in acute Stanford Type A aortic dissection with Doppler renal resistive index. *J Ultrasound Med Off J Am Inst Ultrasound Med*. 2017;36:2105-2111.
- Alfson DB, Ham SW. Type B aortic dissections: current guidelines for treatment. *Cardiol Clin*. 2017;35(3):387-410. [CrossRef]
- Del Porto F, Di Gioia C, Tritapepe L, et al. The multitasking role of macrophages in Stanford type A acute aortic dissection. *Cardiology*. 2014;127(2):123-129. [CrossRef]
- Del Porto F, Proietta M, Tritapepe L, et al. Inflammation and immune response in acute aortic dissection. *Ann Med*. 2010;42(8):622-629. [CrossRef]
- Balch WE, Morimoto RI, Dillin A, Kelly JW. Adapting proteostasis for disease intervention. *Science*. 2008;319(5865):916-919. [CrossRef]
- Hurtley SM, Bole DG, Hoover-Litty H, Helenius A, Copeland CS. Interactions of misfolded influenza virus hemagglutinin with binding protein (BiP). *J Cell Biol*. 1989;108(6):2117-2126. [CrossRef]
- Smith MH, Ploegh HL, Weissman JS. Road to ruin: targeting proteins for degradation in the endoplasmic reticulum. *Science*. 2011;334(6059):1086-1090. [CrossRef]
- Travers KJ, Patil CK, Wodicka L, Lockhart DJ, Weissman JS, Walter P. Functional and genomic analyses reveal essential

- coordination between the unfolded protein response and endoplasmic reticulum-associated degradation. *Cell*. 2000;101(3):249-258.
11. Wang L, Song R, Ma M, et al. Inhibition of autophagy can promote the apoptosis of bladder cancer cells induced by SC66 through the endoplasmic reticulum stress pathway. *Chem Biol Interact*. 2023;384:110725. [CrossRef]
 12. Choi SW, Cho W, Oh H, et al. Madecassoside ameliorates hepatic steatosis in high-fat diet-fed mice through AMPK/autophagy-mediated suppression of ER stress. *Biochem Pharmacol*. 2023;217:115815. [CrossRef]
 13. Zhu X, Chen X, Shen X, et al. PP4R1 accelerates the malignant progression of NSCLC via up-regulating HSPA6 expression and HSPA6-mediated ER stress. *Biochim Biophys Acta Mol Cell Res*. 2023;1871(1):119588. [CrossRef]
 14. Zhu Z, Pu J, Li Y, et al. RBM25 regulates hypoxic cardiomyocyte apoptosis through CHOP-associated endoplasmic reticulum stress. *Cell Stress Chaperones*. 2023;28(6):861-876. [CrossRef]
 15. Zhao Y, Liu Y, Deng J, et al. Ginsenoside F4 alleviates skeletal muscle insulin resistance by regulating PTP1B in type II diabetes mellitus. *J Agric Food Chem*. 2023;71(39):14263-14275. [CrossRef]
 16. Qiang, Zhu, Runmin, et al. Endoplasmic reticulum stress-mediated apoptosis contributing to high glucose-induced vascular smooth muscle cell calcification. *J Vasc Res*. 2016;52(5):291.
 17. Pan S, Wu D, Teschendorff AE, et al. JAK2-centered interactome hotspot identified by an integrative network algorithm in acute Stanford Type A aortic dissection. *PLoS One*. 2014;9(2):e89406. [CrossRef]
 18. Zhou Z, Liu Y, Zhu X, et al. Exaggerated autophagy in Stanford Type A aortic dissection: a transcriptome pilot analysis of human ascending aortic tissues. *Genes*. 2020;11(10):1187. [CrossRef]
 19. Villanueva RAM, Chen ZJ. ggplot2: Elegant Graphics for Data Analysis (2nd ed.). Measurement Interdisciplinary Research & Perspectives 2019; 17(3): 160-67.DOI:10.1080/15366367.2019.1565254.
 20. Gu Z, Eils R, Schlesner M. Complex heatmaps reveal patterns and correlations in multidimensional genomic data. *Bioinformatics*. 2016;32(18):2847-2849. [CrossRef]
 21. Deng B, Liao F, Liu Y, et al. Comprehensive analysis of endoplasmic reticulum stress-associated genes signature of ulcerative colitis. *Front Immunol*. 2023;14:1158648. [CrossRef]
 22. Franz M, Rodriguez H, Lopes C, et al. GeneMANIA update 2018. *Nucleic Acids Res*. 2018;46:W60-W64. [CrossRef]
 23. Chen B, Khodadoust MS, Liu CL, Newman AM, Alizadeh AA. Profiling tumor infiltrating immune cells with CIBERSORT. *Methods Mol Biol*. 2018;1711:243-259. [CrossRef]
 24. Zhou G, Soufan O, Ewald J, Hancock REW, Basu N, Xia J. NetworkAnalyst 3.0: a visual analytics platform for comprehensive gene expression profiling and meta-analysis. *Nucleic Acids Res*. 2019;47:W234-W241. [CrossRef]
 25. Team RDC. R: A language and environment for statistical computing. R Foundation for Statistical Computing: Vienna, Austria. *Computing*. 2009;14:12-21.
 26. Chen H, Luo S, Chen H, Zhang C. ATF3 regulates SPHK1 in cardiomyocyte injury via endoplasmic reticulum stress. *Immun Inflamm Dis*. 2023;11(9):e998. [CrossRef]
 27. Zhou F, Gao H, Shang L, et al. Oridonin promotes endoplasmic reticulum stress via TP53-repressed TCF4 transactivation in colorectal cancer. *J Exp Clin Cancer Res*. 2023;42(1):150. [CrossRef]
 28. Song L, Alcalai R, Arad M, et al. Calsequestrin 2 (CASQ2) mutations increase expression of calreticulin and ryanodine receptors, causing catecholaminergic polymorphic ventricular tachycardia. *J Clin Invest*. 2007;117:1814-1823. [CrossRef]
 29. Valle G, Arad M, Volpe P. Molecular adaptation to calsequestrin 2 (CASQ2) point mutations leading to catecholaminergic polymorphic ventricular tachycardia (CPVT): comparative analysis of R33Q and D307H mutants. *J Muscle Res Cell Motil*. 2020; 41(2-3):251-258. [CrossRef]
 30. Chen H, Valle G, Furlan S, et al. Mechanism of calsequestrin regulation of single cardiac ryanodine receptor in normal and pathological conditions. *J Gen Physiol*. 2013;142(2):127-136. [CrossRef]
 31. Hamilton S, Terentyev D. Altered intracellular calcium homeostasis and arrhythmogenesis in the aged heart. *Int J Mol Sci*. 2019;20(10). [CrossRef]
 32. Wang SK, Green LA, Gutwein AR, et al. Osteopontin may be a driver of abdominal aortic aneurysm formation. *J Vasc Surg*. 2018;68(6S):225-295. [CrossRef]
 33. Waller AH, Sanchez-Ross M, Kaluski E, Klapholz M. Osteopontin in cardiovascular disease: a potential therapeutic target. *Cardiol Rev*. 2010;18(3):125-131. [CrossRef]
 34. Clemente N, Raineri D, Cappellano G, et al. Osteopontin bridging innate and adaptive immunity in autoimmune diseases. *J Immunol Res*. 2016;13:1-15.
 35. Yushi Q, Li Z, Von Roemeling CA, et al. Osteopontin is a multifaceted pro-tumorigenic driver for central nervous system lymphoma. *Oncotarget*. 2016;7(22):32156-32171.
 36. Arif EM, Makhbule GK. The multiple functions and mechanisms of osteopontin. *Clin Biochem*. 2018;59:S0009912018303837.
 37. Freiholtz D, Bergman O, Pradhananga S, Lng K, Poujade FA, Granath C, et al. SPP1/osteopontin: a driver of fibrosis and inflammation in degenerative ascending aortic aneurysm? *Journal of Molecular Medicine*. 2023;101(10):1323-33.
 38. Inada K, Koga M, Yamada A, Dohgu S, Yamauchi A. Moxifloxacin induces aortic aneurysm and dissection by increasing osteopontin in mice. *Biochem Biophys Res Commun*. 2022;629:1-5. [CrossRef]
 39. Mao H, Chen W, Chen L, Li L. Potential role of mitochondria-associated endoplasmic reticulum membrane proteins in diseases. *Biochem Pharmacol*. 2022;199:115011. [CrossRef]
 40. Ji C, Wang X, Xue B, et al. A fluorescent Nano vector for early diagnosis and enhanced interleukin-33 therapy of thoracic aortic dissection. *Biomaterials*. 2023;293:121958. [CrossRef]
 41. Yang X, Xu C, Yao F, et al. Targeting endothelial tight junctions to predict and protect thoracic aortic aneurysm and dissection. *Eur Heart J*. 2023;44(14):1248-1261. [CrossRef]
 42. Rao Z, Zheng Y, Xu L, et al. Endoplasmic reticulum stress and pathogenesis of vascular calcification. *Front Cardiovasc Med*. 2022;9:918056. [CrossRef]
 43. Kurihara T, Shimizu-Hirota R, Shimoda M, et al. Neutrophil-derived matrix metalloproteinase 9 triggers acute aortic dissection. *Circulation*. 2012;126(25):3070-3080. [CrossRef]
 44. Tyrrell DJ, Goldstein DR. Ageing and atherosclerosis: vascular intrinsic and extrinsic factors and potential role of IL-6. *Nat Rev Cardiol*. 2021;18(1):58-68. [CrossRef]
 45. Zhao A, Fan Q, Qijue L, et al. Interleukin-6 downregulated vascular smooth muscle cell contractile proteins via ATG4B-mediated autophagy in thoracic aortic dissection. *Heart Vessels*. 2017;32(12):1523-1535. (doi:[CrossRef])
 46. Ait-Oufella H, Wang Y, Herbin O, et al. Natural regulatory T cells limit angiotensin II-induced aneurysm formation and rupture in mice. *Arterioscler Thromb Vasc Biol*. 2013;33(10):2374-2379. [CrossRef]
 47. Zhang X, Che Y, Mao L, et al. H3.3B controls aortic dissection progression by regulating vascular smooth muscle cells phenotypic transition and vascular inflammation. *Genomics*. 2023; 115(5):110685. [CrossRef]

Supplementary File S1

	A	B	C	D	E	F	G	H
1	id	logFC	AveExpr	t	P.Value	adj.P.Val	B	gene
2	ILMN_1760798	-2,4615297	6,19563705	-8,5457042	2,03771E-06	0,01637688	5,00240335	RYR2
3	ILMN_1733746	-3,6678588	7,44938102	-7,9165954	4,45565E-06	0,02508415	4,35572849	REEP1
4	ILMN_1683178	-1,7785296	7,54176565	-7,2192142	1,11831E-05	0,02576853	3,57325451	JAK2
5	ILMN_1658660	-5,1444348	8,30373674	-7,0609975	1,38935E-05	0,02576853	3,38556748	ACTC1
6	ILMN_1664630	2,99801227	4,61196009	6,74867397	2,15241E-05	0,02576853	3,00358631	CHEK1
7	ILMN_1651354	3,79791129	9,04558845	6,57872372	2,74595E-05	0,02739081	2,78920511	SPP1
8	ILMN_1666305	3,86285789	5,68129689	6,50487439	3,05612E-05	0,02861835	2,69459382	CDKN3
9	ILMN_1751028	2,05872208	9,25308534	6,16710813	5,0329E-05	0,03139493	2,2504848	SERPINH1
10	ILMN_1809695	-1,7393782	9,05249039	-5,6752249	0,000107036	0,03935819	1,56985111	CAMK2G
11	ILMN_1759023	-1,3206888	9,59524765	-5,4874055	0,00014406	0,04165051	1,29928529	WFS1
12	ILMN_1722329	-4,0428139	6,93625584	-5,3357639	0,000183774	0,04632685	1,07654924	CASQ2
13	ILMN_1770758	-3,1371289	4,01725748	-7,8393135	4,92007E-06	0,02508415	4,27251278	AKAP6
14	ILMN_3248541	3,67110687	3,58313356	14,3549927	7,23826E-09	0,00033213	9,02013753	LOC100132429
15	ILMN_1687978	2,76325256	8,35170973	9,51219287	6,63508E-07	0,01522253	5,89662226	PHLDA1
16	ILMN_1809590	4,35098376	5,51874302	9,02124703	1,1598E-06	0,01637688	5,45668044	GIN52
17	ILMN_1792455	3,47414514	8,07941283	8,73475091	1,62421E-06	0,01637688	5,18643047	TMEM158
18	ILMN_1747744	1,37263577	8,71840828	7,48641584	7,80633E-06	0,02576853	3,88155811	LHFPL2
19	ILMN_1723134	-2,8421983	3,82717223	-7,4660453	8,02076E-06	0,02576853	3,8584321	LOC650695
20	ILMN_1791726	5,13319432	6,70652317	7,4030037	8,72518E-06	0,02576853	3,78647039	TUBB3
21	ILMN_1717173	2,35873639	5,99305189	7,32884813	9,63934E-06	0,02576853	3,70105792	ECT2
22	ILMN_1706643	2,11244695	11,9680205	7,24045993	1,08645E-05	0,02576853	3,59816441	COL6A3
23	ILMN_1743939	-1,6548923	7,22174145	-7,2094563	1,13327E-05	0,02576853	3,56179065	C5ORF24
24	ILMN_1810054	-3,4951422	9,66699232	-7,1965594	1,15338E-05	0,02576853	3,54661647	CNN1
25	ILMN_1663390	4,1570673	6,77274127	7,17771071	1,18346E-05	0,02576853	3,52439371	CDC20
26	ILMN_1708743	2,53403997	7,7383859	7,11376735	1,29189E-05	0,02576853	3,44859632	NT5DC2
27	ILMN_1691790	-3,3142387	2,72992803	-7,1040352	1,3093E-05	0,02576853	3,4370046	DACT2
28	ILMN_1711566	1,18982727	13,7630262	7,09536697	1,32501E-05	0,02576853	3,42666777	TIMP1
29	ILMN_1758852	3,61637755	2,88389907	7,01958451	1,47132E-05	0,02576853	3,33580023	ENTPD7
30	ILMN_1747911	2,89060725	5,54023976	6,94317335	1,63641E-05	0,02576853	3,24327093	CDC2
31	ILMN_1691410	-2,2251432	9,15804562	-6,9149198	1,70236E-05	0,02576853	3,20882544	BAMBI
32	ILMN_1670238	4,33821096	5,08100305	6,87602244	1,79782E-05	0,02576853	3,16119744	CDC45L
33	ILMN_1811997	-1,4792279	9,94022597	-6,8697467	1,81375E-05	0,02576853	3,15349064	ZNF364

	A	B	C	D	E	F	G	H
34	ILMN_1726352	-1,9345496	4,81862682	-6,8560297	1,8491E-05	0,02576853	3,13662421	THSD4
35	ILMN_1741165	4,63056961	5,28932665	6,81904807	1,94809E-05	0,02576853	3,09100272	SLC11A1
36	ILMN_2049021	3,11439351	6,82569756	6,81561865	1,95755E-05	0,02576853	3,08676109	PTTG3P
37	ILMN_3294365	2,78451177	4,09415041	6,77322088	2,07866E-05	0,02576853	3,0341674	LOC646993
38	ILMN_1741801	1,91719772	5,63922358	6,75616718	2,12961E-05	0,02576853	3,01293172	CDC7
39	ILMN_1783120	-2,3617011	10,4106065	-6,7506996	2,14622E-05	0,02576853	3,0061135	SLMAP
40	ILMN_1665792	2,35334239	7,18064476	6,73643917	2,1902E-05	0,02576853	2,98830795	ITGA2
41	ILMN_2136971	-3,04402	3,81932673	-6,6747994	2,39164E-05	0,02598744	2,91096959	FABP3
42	ILMN_1784948	4,30166224	5,91067784	6,67428856	2,39339E-05	0,02598744	2,91032605	SPOCD1
43	ILMN_1800911	-3,4752269	3,9019519	-6,6669212	2,41878E-05	0,02598744	2,90104085	FLJ10324
44	ILMN_1697338	-3,4416194	4,29301564	-6,6621565	2,43535E-05	0,02598744	2,89503128	SRPK3
45	ILMN_1799028	1,45087395	7,65400636	6,62620533	2,56434E-05	0,02637496	2,84956864	TSPAN5
46	ILMN_1657547	1,91397508	8,56573	6,62018874	2,58663E-05	0,02637496	2,8419399	CCDC34
47	ILMN_1699071	-2,0836157	8,72588901	-6,5554632	2,83986E-05	0,0277249	2,75950075	C21ORF7
48	ILMN_1677719	1,97021909	6,81822808	6,53875206	2,90944E-05	0,02781243	2,73810585	CHST1
49	ILMN_2412281	-1,7620139	7,58556079	-6,4653833	3,23709E-05	0,02970674	2,64363602	PDLIM5
50	ILMN_2367883	-2,6545286	9,59757488	-6,4271407	3,42322E-05	0,03020351	2,59404652	GEM
51	ILMN_2212909	4,01350045	5,47365088	6,42231901	3,44749E-05	0,03020351	2,58777721	MELK
52	ILMN_1786065	2,73360743	7,64297585	6,41421314	3,48869E-05	0,03020351	2,57722912	UHRF1
53	ILMN_1761322	-1,811963	7,31072294	-6,3954873	3,58589E-05	0,03023486	2,55282027	FHOD3
54	ILMN_1653856	2,6712773	5,64170313	6,37520953	3,69441E-05	0,03027104	2,52632354	STS-1
55	ILMN_2075603	-1,9570636	7,9818311	-6,3570321	3,79465E-05	0,0305469	2,50251397	MRGPRF
56	ILMN_1869943	-1,6998345	4,29699189	-6,314243	4,04219E-05	0,03139493	2,44625244	HS.445239
57	ILMN_1664516	3,20139449	5,24990302	6,30276043	4,1115E-05	0,03139493	2,43110316	CENPF
58	ILMN_1682015	2,98798905	4,68515835	6,29941653	4,13192E-05	0,03139493	2,42668738	GAL
59	ILMN_2042771	2,76889721	7,95529123	6,21398705	4,69188E-05	0,03139493	2,31324751	PTTG1
60	ILMN_2050911	2,622241	5,34427592	6,21218727	4,70451E-05	0,03139493	2,31084464	SLC22A4
61	ILMN_2051373	3,02763669	4,38947209	6,19535521	4,82438E-05	0,03139493	2,28834634	NEK2
62	ILMN_1725791	-1,9686818	9,00354111	-6,1904053	4,86025E-05	0,03139493	2,28172122	PTPLA
63	ILMN_1724941	3,10171677	4,71519934	6,16829973	5,02392E-05	0,03139493	2,25208466	CDCP1
64	ILMN_1712532	1,83554963	6,35213414	6,16127372	5,07715E-05	0,03139493	2,24264804	CARD9
65	ILMN_3247728	-1,7444317	8,35691515	-6,1585491	5,09796E-05	0,03139493	2,23898644	RNF115
66	ILMN_1783276	-2,5788459	10,2944696	-6,1511878	5,15462E-05	0,03139493	2,2290873	NEXN

	A	B	C	D	E	F	G	H
67	ILMN_1655191	-1,2374161	6,69832958	-6,1365657	5,26917E-05	0,03139947	2,20939761	CASZ1
68	ILMN_1672662	1,54629645	9,58261376	6,08848555	5,66525E-05	0,03332694	2,1444038	SLC20A1
69	ILMN_1717393	2,15869765	4,21330406	6,06315216	5,88654E-05	0,03412881	2,11000384	PTCHD1
70	ILMN_1709026	-1,5348391	6,96916297	-6,0143823	6,33877E-05	0,03412881	2,0434786	C6ORF145
71	ILMN_1796589	3,00074329	6,1474078	6,00933263	6,38765E-05	0,03412881	2,03656791	TRIP13
72	ILMN_3244019	-2,0000166	9,90400525	-5,9912084	6,56643E-05	0,03412881	2,01172895	LOC647886
73	ILMN_1793360	1,3971315	6,30115709	5,971879	6,76295E-05	0,03412881	1,98517784	APITD1
74	ILMN_1725534	-1,839644	10,6926597	-5,9658939	6,82505E-05	0,03412881	1,97694394	ACTN4
75	ILMN_1658289	1,38471016	8,39163172	5,95780382	6,90996E-05	0,03412881	1,96580475	WDR54
76	ILMN_1711470	2,56945632	6,43595763	5,94126965	7,087E-05	0,03423022	1,94300482	UBE2T
77	ILMN_2392274	1,7923068	7,54721682	5,93149616	7,19391E-05	0,03432084	1,9295061	CD82
78	ILMN_1695658	5,30820897	5,26588183	5,92594716	7,25536E-05	0,03432084	1,92183496	KIF20A
79	ILMN_2362549	4,62033121	4,20887021	5,91520494	7,37591E-05	0,03453508	1,90696988	ZWINT
80	ILMN_1743836	-1,1998589	10,1608574	-5,9004161	7,54537E-05	0,03462191	1,88647349	MXRA7
81	ILMN_1663575	2,40702133	8,7126013	5,88332102	7,74639E-05	0,03490025	1,8627353	MGC87042
82	ILMN_1677200	-2,2269251	9,33385153	-5,8823359	7,75815E-05	0,03490025	1,86136593	CYFIP2
83	ILMN_1671478	-2,6632185	6,70213225	-5,87336	7,86613E-05	0,03504248	1,84888087	CKB
84	ILMN_1801939	4,73012912	5,22257181	5,86529464	7,96453E-05	0,03510284	1,83765091	CCNB2
85	ILMN_2071446	4,22232857	6,86970229	5,84578856	8,20791E-05	0,03510284	1,8104462	PI15
86	ILMN_2041725	-3,3790076	5,48577205	-5,8432796	8,23978E-05	0,03510284	1,80694241	MYOZ2
87	ILMN_1683450	3,45322602	6,32725227	5,84186769	8,25778E-05	0,03510284	1,80497016	CDCA5
88	ILMN_1737205	2,37013726	7,21639205	5,82686141	8,45161E-05	0,03557817	1,78398803	MCM4
89	ILMN_2311537	2,54256683	7,31882998	5,81264402	8,6397E-05	0,03603932	1,76407417	HMGA1
90	ILMN_1684211	3,94446674	3,60012749	5,79895977	8,82492E-05	0,03639992	1,7448751	SEC14L2
91	ILMN_3239254	-2,4129725	4,77374898	-5,7942554	8,88957E-05	0,03639992	1,73826766	UCA1
92	ILMN_1697189	-4,3116805	5,35552788	-5,7658143	9,2912E-05	0,03655563	1,69824186	PNCK
93	ILMN_1806040	2,7227556	7,95311123	5,76557615	9,29465E-05	0,03655563	1,69790618	TYMS
94	ILMN_2082585	1,82810276	9,062173	5,7637462	9,32115E-05	0,03655563	1,69532616	SNAI2
95	ILMN_1808071	2,19366761	5,26457225	5,71387219	0,000100751	0,03884833	1,62479325	KIF14
96	ILMN_1684217	4,86158448	4,16665416	5,69967353	0,000103013	0,0390316	1,60463705	AURKB
97	ILMN_1776105	1,21731937	5,29245309	5,68634111	0,000105187	0,0392397	1,58567981	PSPH
98	ILMN_1881005	-2,5161237	4,89404957	-5,6741297	0,00010722	0,03935819	1,56829038	HS.560387
99	ILMN_3284000	-2,7449175	4,81042881	-5,6607282	0,000109499	0,03946133	1,54917761	LOC100131857

	A	B	C	D	E	F	G	H
100	ILMN_1680344	-2,4731055	8,52165084	-5,6595919	0,000109694	0,03946133	1,54755571	MYOM1
101	ILMN_1706969	2,3596389	5,66131692	5,65735431	0,000110081	0,03946133	1,54436114	BEND6
102	ILMN_1738095	-2,0295929	8,3771417	-5,6366707	0,00011372	0,03992537	1,51479208	PER2
103	ILMN_1727055	2,9686162	4,91172789	5,63518763	0,000113985	0,03992537	1,51266921	C12ORF48
104	ILMN_1733094	2,37788398	7,68216967	5,62057293	0,00011664	0,04036352	1,49172948	STEAP1
105	ILMN_1696187	1,36475645	8,64329079	5,6146288	0,000117738	0,04036352	1,48320259	PYGL
106	ILMN_1710954	1,58594753	5,90853279	5,61274531	0,000118088	0,04036352	1,48049947	LOC283932
107	ILMN_1660986	-2,520449	6,37683292	-5,6077395	0,000119025	0,04036352	1,47331244	PER3
108	ILMN_1742145	3,57039029	3,40300836	5,60449946	0,000119635	0,04036352	1,46865839	ESPL1
109	ILMN_1774207	1,99588226	8,70217905	5,59103283	0,000122206	0,04093024	1,44929579	ANGPT2
110	ILMN_1785618	-1,2791962	9,75954004	-5,5789606	0,000124562	0,04118814	1,43191229	SMTN
111	ILMN_1738578	-2,3552381	11,0480003	-5,5759495	0,000125156	0,04118814	1,42757275	FILIP1L
112	ILMN_1669550	1,36020255	8,64384992	5,55894789	0,000128572	0,04154592	1,40304131	MAD2L2
113	ILMN_1811921	-1,3194005	11,8656567	-5,5508176	0,00013024	0,04163871	1,39129312	CSRP1
114	ILMN_2315979	-1,5313465	9,4750145	-5,5473085	0,000130967	0,04163871	1,38621924	LBH
115	ILMN_1686664	2,70257225	11,9639799	5,54435786	0,000131581	0,04163871	1,38195109	MT2A
116	ILMN_1661197	2,26060629	6,19984026	5,53633826	0,000133267	0,04165051	1,37034345	CLCF1
117	ILMN_2405353	-1,3194265	4,36361438	-5,5349246	0,000133567	0,04165051	1,36829626	SDK1
118	ILMN_2355665	2,888197	6,29547682	5,52947992	0,000134727	0,04165051	1,36040811	MTP18
119	ILMN_1779448	-2,5352459	10,8403908	-5,5226529	0,000136197	0,04165051	1,35051041	EFHD1
120	ILMN_1780667	2,31684624	5,76365601	5,51579356	0,000137691	0,04165051	1,34055791	WDR51A
121	ILMN_1772316	-1,3905522	9,16481712	-5,5029216	0,000140541	0,04165051	1,32186043	UNC84A
122	ILMN_2196984	2,34581395	5,47005138	5,50164744	0,000140827	0,04165051	1,32000806	OIP5
123	ILMN_1752935	-2,4535718	7,92147286	-5,5000647	0,000141182	0,04165051	1,31770671	TMEM30B
124	ILMN_1737184	2,03697969	6,35982823	5,49563108	0,000142183	0,04165051	1,31125809	CDCA7
125	ILMN_1756049	-1,814194	9,02354281	-5,4866458	0,000144235	0,04165051	1,29817901	NT5DC3
126	ILMN_1719695	1,33505066	9,64571258	5,47971059	0,00014584	0,04165051	1,28807482	NFKBIZ
127	ILMN_2160929	2,4590368	7,85550506	5,47841261	0,000146142	0,04165051	1,28618285	FEN1
128	ILMN_1811470	2,33197555	4,18483263	5,4458738	0,000153944	0,04330887	1,23866187	PLEK2
129	ILMN_2173611	1,55719823	11,5274272	5,44025281	0,000155336	0,04330887	1,23043491	MT1E
130	ILMN_2189675	-3,0354289	6,52476637	-5,4386466	0,000155736	0,04330887	1,22808307	HRCT1
131	ILMN_1795325	-1,8432437	12,2255004	-5,4124713	0,000162413	0,04438365	1,18969646	ACTG2
132	ILMN_1800412	1,38667231	8,44671746	5,41212453	0,000162503	0,04438365	1,18918713	BMP1

	A	B	C	D	E	F	G	H
133	ILMN_3236821	-1,2198729	9,62540265	-5,3993064	0,000165884	0,04454153	1,17034689	HSPBL2
134	ILMN_1760493	-1,8293931	8,71590243	-5,3988963	0,000165993	0,04454153	1,16974366	LIMS2
135	ILMN_1681503	2,62458991	5,5624888	5,36256733	0,000175991	0,04599013	1,11619633	MCM2
136	ILMN_1735093	2,04111471	6,66832232	5,35778251	0,000177355	0,04599013	1,10912743	TIMELESS
137	ILMN_2143795	1,65221644	9,67882535	5,35428931	0,000178357	0,04599013	1,10396432	MGC4677
138	ILMN_3292122	-1,5398862	2,99483388	-5,353391	0,000178616	0,04599013	1,10263626	LOC100133263
139	ILMN_1773119	2,55323454	6,01681582	5,34843483	0,000180051	0,04599013	1,09530662	CCNF
140	ILMN_1653319	1,32745651	6,71397411	5,34777379	0,000180243	0,04599013	1,0943287	MC1R
141	ILMN_1698706	3,00738937	5,79487319	5,34719131	0,000180412	0,04599013	1,09346695	NID2
142	ILMN_1689378	1,98997535	5,14302393	5,34176421	0,000182001	0,04613868	1,08543507	CCRN4L
143	ILMN_3206352	-1,8370337	3,80651287	-5,332446	0,000184762	0,04632685	1,07163315	LOC728264
144	ILMN_2077550	1,82001804	7,00660088	5,3196079	0,000188639	0,04640748	1,05259424	RACGAP1
145	ILMN_1766707	-2,6455528	4,01520244	-5,3192753	0,000188741	0,04640748	1,05210059	IL17B
146	ILMN_1707356	-1,0099326	6,23293698	-5,3143064	0,000190265	0,04640748	1,04472417	CFL2
147	ILMN_3310065	2,72944318	3,15853947	5,31143537	0,000191152	0,04640748	1,04046018	SFTA1P
148	ILMN_2072296	2,42210817	8,13392393	5,30045058	0,000194585	0,04643182	1,02413331	CKS2
149	ILMN_1807169	-2,3208483	6,93596679	-5,2981971	0,000195297	0,04643182	1,02078147	TINAGL1
150	ILMN_1784113	1,27756752	6,70439922	5,29791189	0,000195388	0,04643182	1,02035717	NAT14
151	ILMN_1732452	1,44832794	8,81488705	5,29422416	0,00019656	0,04643182	1,01487004	MAPKAPK3
152	ILMN_2368718	4,24674121	4,65719652	5,29183298	0,000197324	0,04643182	1,0113109	CENPM
153	ILMN_3244640	2,8153156	4,1346459	5,28069323	0,000200924	0,04703784	0,99471761	SNORD96A
154	ILMN_1880457	1,39210596	7,47372222	5,26229834	0,000207022	0,04791322	0,96727267	HS.556994
155	ILMN_1700771	-1,9426405	7,8027402	-5,2618295	0,00020718	0,04791322	0,96657249	PRUNE2
156	ILMN_1687556	-3,3355393	4,2650239	-5,2591269	0,000208093	0,04791322	0,96253523	DAPL1
157	ILMN_1720124	1,17225141	9,57394502	5,25617361	0,000209096	0,04791322	0,95812231	RCC2
158	ILMN_2199362	-3,5280798	3,78818573	-5,2504857	0,000211041	0,04791322	0,94961899	FBXL22
159	ILMN_1757020	-2,4758747	3,74344829	-5,2477785	0,000211973	0,04791322	0,94556999	CDH8
160	ILMN_1776490	2,22117304	4,97308462	5,23842273	0,000215229	0,04841069	0,93156768	C17ORF53
161	ILMN_1684143	-2,4936743	3,86584964	-5,2308518	0,000217902	0,04877291	0,92022608	NPTXR